Journal of Chromatography A 1741 (2025) 465602

Contents lists available at ScienceDirect

Journal of Chromatography A

journal homepage: www.elsevier.com/locate/chroma

Mechanistic modeling of anti-Langmuirian to Langmuirian behavior of Fc-fusion proteins in cation exchange chromatography

Yu-Cheng Chen [a,b], Xue-Zhao Zhong [c], Ce Shi [c], Ran Chen [c], Mattia Sponchioni [b], Shan-Jing Yao [a], Dong-Qiang Lin [a,*]

[a] Key Laboratory of Biomass Chemical Engineering of Ministry of Education, Zhejiang Key Laboratory of Smart Biomaterials, College of Chemical and Biological Engineering, Zhejiang University, Hangzhou 310058, China
[b] Department of Chemistry, Materials and Chemical Engineering, Politecnico di Milano, Via Mancinelli 7 20131 Milano, Italy
[c] Shanghai Engineering Research Center of Anti-tumor Biological Drugs, Shanghai Henlius Biotech, Inc., Shanghai, China

ARTICLE INFO

Keywords:
ion-exchange chromatography
mechanistic model
anti-Langmuirian to Langmuirian behavior
process optimization
Fc-fusion protein
thermodynamic model

ABSTRACT

Development of a next-generation chromatographic model, capable of simultaneously meeting academic demands for thermodynamic consistency and industrial requirements in everyday project work, has become a focal point of research. In this study, anti-Langmuirian to Langmuirian (AL-L) elution behavior was observed in cation-exchange chromatographic separation of charge variants of industrial Fc-fusion proteins. To characterize this behavior, the multi-protein Mollerup activity model was integrated into the steric mass action (SMA) model, resulting in a new model named the generalized ion-exchange (nGIEX) isotherm for multi-protein systems. An R^2 exceeding 0.95 calibrated by three elution experiments indicates an effective description of the AL-L behavior (dynamic adsorption). Using isotherm sampling, the nGIEX model exhibited sigmoidal AL-L isotherms (static adsorption). Finally, the model's extrapolation capability was externally validated through process optimization, resulting in an optimal two-step elution condition and a yield improvement of the main variant from 25.9 % to 89.1 % within purity specifications (>70 %).

1. Introduction

Chromatographic modeling originated in the 1980s [1,2]. In recent years, propelled by advancements in computer simulation techniques [3], chromatographic modeling has expanded into increasingly diverse application scenarios [4–14]. These applications have imposed new demands on the expression of chromatographic models [15–22]. Development of a next-generation chromatographic model, capable of simultaneously meeting academic demands for thermodynamic consistency and industrial requirements in everyday project work, has become a focal point of research [23,24]. The thermodynamic consistency refers to the requirement that the chromatographic model adhere to the laws of thermodynamics. This consistency ensures that the model produce results that are physically plausible.

Equilibrium isotherms are one of pivotal aspects of thermodynamic consistency in chromatographic modeling. The chromatographic model should accurately describe systems at equilibrium. The first row in Fig. 1 illustrates four classical types of adsorption isotherms: linear, Langmuirian, anti-Langmuirian, and sigmoid (also known as anti-Langmuirian to Langmuirian, AL-L). The second and third rows depict their first and second derivatives, respectively. The final row illustrates their corresponding elution curves under conditions of axial dispersion as loadings increase in a single-component system. Typically, the linear model is only applicable at low mobile-phase concentration, thus lacking practical significance. Currently, the most widely-used adsorption model is Langmuirian isotherm, such as a steric mass action (SMA) model for ion exchange chromatography [25] and a Langmuir model for protein A chromatography. Compared to the Langmuirian isotherm, the anti-Langmuirian is convex (with first and second derivatives consistently greater than zero). Traditionally, the binding between proteins and ligands should adhere to the Langmuirian isotherm [26,27].

However, recent studies have observed a more complex adsorption process: anti-Langmuirian adsorption at lower loadings and Langmuirian adsorption at higher loadings for static adsorption [28,29]. This transition manifests in the elution profiles (dynamic adsorption) of cation exchange chromatography as species eluted earlier exhibit the Langmuirian adsorption, whereas those eluted later exhibit the anti-Langmuirian adsorption. Such AL-L transition corresponds to a

* Corresponding author at: College of Chemical and Biological Engineering, Zhejiang University, Hangzhou 310058, China.
E-mail address: lindq@zju.edu.cn (D.-Q. Lin).

https://doi.org/10.1016/j.chroma.2024.465602
Received 12 November 2024; Received in revised form 6 December 2024; Accepted 15 December 2024
Available online 16 December 2024

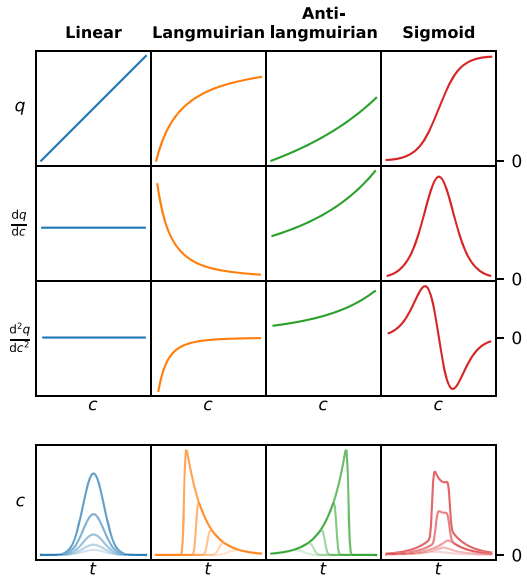

Fig. 1. Relationship between equilibrium isotherms and under conditions of axial dispersion for single components as loadings increase. Linear: $\frac{\partial q_i}{\partial c_i} = \text{const}$ and $\frac{\partial^2 q}{\partial c_i^2} = 0$; Langmuirian: $\frac{\partial q_i}{\partial c_i} > 0$ and $\frac{\partial^2 q}{\partial c_i^2} < 0$; anti-Langmuirian: $\frac{\partial q_i}{\partial c_i} > 0$ and $\frac{\partial^2 q}{\partial c_i^2} > 0$; sigmoid: $\frac{\partial q_i}{\partial c_i} > 0$ and $\exists c_0$ such that $\frac{\partial^2 q}{\partial c_i^2}(c_0) = 0$.

sigmoidal shape in their isotherm, thereby the sigmoidal isotherm is termed as the AL-L isotherm.

The AL-L behavior was first observed by Mihlbachler, et al. [28] in the separation of (±)-Tröger's base enantiomers with a silica-based packing column. Khalaf, et al. [29] also observed this AL-L behavior in the polyelectrolyte brush type cation-exchangers. Both Mihlbachler, et al. [28] and Khalaf, et al. [29] attributed this AL-L behavior to multi-layer adsorption. Khalaf, et al. [29], through comparative observations of different protein elution profiles on various ligands, further explained that the multi-layer adsorption arises from the thorough utilization of the polyelectrolyte brush's 3D structure by proteins. Thus, the AL-L behavior occurs only when proteins can fully use the polyelectrolyte brush's 3D structure.

Another theory of multi-layer adsorption is protein self-association developed by Mollerup, et al. [30]. They proposed that a protein molecule can function as a ligand and associate with another protein molecule, forming a double layer. To describe this adsorption behavior, they introduced a self-association (SAS) isotherm model based on applied thermodynamics. The SAS model is a kind of sigmoid isotherms that can describe AL-L behavior [31–33]. Additionally, the SAS model ensures the thermodynamic consistency and can be used to describe various chromatographic processes beyond ion exchange chromatography, such as hydrophobic interaction chromatography [34], mixed-mode chromatography [35–38], reversed-phase chromatography [39,40]. However, the SAS model introduces numerous model parameters to be calibrated, thereby increasing the effort of calibration experiments and sample losses [31–33]. This approach is not economically viable for high-value bioproducts, such as monoclonal antibodies and Fc-fusion proteins.

Vetter and Strube [23] argued that the next-generation chromatographic models must not only meet academic demands for thermodynamic consistency but also fulfill industrial requirements in everyday project work. These industrial requirements include: the model's ability to describe adsorption processes commonly encountered in industrial applications, and minimizing the number of model parameters while ensuring accuracy. Both Langmuirian and anti-Langmuirian adsorptions are frequently encountered in industrial applications. Therefore, the next-generation chromatographic models must be able to describe both behaviors simultaneously. In industrial applications, to ensure productivity, very high loadings are often employed [41]. In such high-loading scenarios, the AL-L behavior becomes more pronounced [29,31,32,42,43] and the solution becomes more non-ideal. Introducing an activity model to correct for the solution non-ideality is essential. Mollerup [44] derived an activity model based on the van der Waals equation of state [45] for single-protein systems, which has been widely applied [34–38].

Industrial applications often involve modeling multiple proteins. Some researchers have introduced the single-protein Mollerup model to multi-protein systems by simply adding subscripts. However, this approach has been proven thermodynamically inconsistent [46]. Therefore, in our previous study [46], a thermodynamically consistent asymmetric activity model was rederived for multi-protein systems and named as the multi-protein Mollerup model. Although this model has been theoretically validated for thermodynamic consistency, its potential in other aspects, such as describing the AL-L behavior, warrants further exploration. This study aims to investigate the application of our previously proposed multi-protein Mollerup model in characterizing the AL-L behavior (dynamic and static adsorption) observed in cation-exchange chromatographic separation of charge variants of industrial Fc-fusion proteins. We would elucidate why the developed model can describe this AL-L behavior through model-based explanations. Finally, the extrapolation capability of the developed model would be confirmed by employing external validation of process optimization.

2. Methods and materials

2.1. Chromatographic models

A chromatographic model consists of the column models for mobile phase c and stationary phase q. In this study the column model used was the equilibrium dispersive model, which considers the contributions from three mass transfer processes: convection (implemented through introducing the superficial velocity u and total porosity ε_t), dispersion (implemented through the apparent axial dispersion coefficient D_{app}), and adsorption (implemented through phase ratio and adsorption kinetics). The column model for protein i at time t and at axial position z is given by:

$$\frac{\partial c_i}{\partial t}(z,t) = -\frac{u}{\varepsilon_t}\frac{\partial c_i}{\partial z}(z,t) + D_{app}\frac{\partial^2 c_i}{\partial z^2}(z,t) - \frac{1-\varepsilon_t}{\varepsilon_t}\frac{\partial q_i}{\partial t}(z,t) \tag{1}$$

which is completed with Danckwerts and Neumann boundary conditions at the column inlet and outlet, respectively:

$$-\frac{\varepsilon_t D_{app}}{u}\frac{\partial c_i}{\partial z}(0,t) + c_i(0,t) = \begin{cases} c_{inj}x_i & 0 < t \le t_{inj} \\ 0 & t > t_{inj} \end{cases} \tag{2}$$

$$\frac{\partial c_i}{\partial z}(L,t) = 0 \tag{3}$$

where t_{inj} and c_{inj} represent the injection time and concentration of proteins, respectively. x_i are the mole fraction of protein i. The difference of the column model between the salt and proteins lies in the absence of the adsorption phase for the salt. Additionally, the boundary conditions at the column inlet for the salt is determined by the elution conditions.

The isotherm model applied was the generalized ion-exchange (nGIEX) isotherm for multi-protein systems (n is the number of proteins, $i,j = 1,2,\cdots,n$):

$$k_{kin,i}\cdot\frac{\partial q_i}{\partial t}(z,t) = k_{eq,i}\cdot\bar{q}_s^{\nu_i}(z,t)\cdot\tilde{\gamma}_i(z,t)\cdot c_i(z,t) - q_i(z,t)\cdot c_s^{\nu_i}(z,t) \tag{4}$$

$$\bar{q}_s(z,t) = \Lambda - \sum_{j=1}^{n}(\nu_j + \sigma_j)\cdot q_j(z,t) \tag{5}$$

$$\ln\tilde{\gamma}(z,t) = k_s c_s(z,t) + k_p \sum_{j=1}^{n} c_j(z,t) \tag{6}$$

$$\frac{\partial q_s}{\partial t}(z,t) = -\sum_{j=1}^{n} \nu_j \cdot \frac{\partial q_j}{\partial t}(z,t) \tag{7}$$

where the salt concentrations are denoted as q_s in the stationary phase and c_s in the mobile phase. $\overline{q}_s$ represents the available sites for binding. Λ is total ion-exchange capacity. This combined model is referred to the generalized ion-exchange (GIEX) isotherm in some literature. However, it must be noted that the activity model, Eq. (6), is the thermodynamically consistent multi-protein Mollerup model, which was proposed in our previous work [46] and whose range lies in (0, 1]. It includes two parameters: k_s for salt-protein interaction and k_p for protein-protein interaction. The summation in Eq. (6) implies that the formula accounts for the contributions of all proteins ($n > 1$) to the solution activity, which is different from the GIEX model reported in the literature that considers the contribution of only a single protein ($n = 1$). To differentiate our model from the reported GIEX model, we referred to our isotherm model as the nGIEX model.

For a single-protein system, the nGIEX model can be degenerated into the GIEX model proposed by Mollerup [44] and Huuk, et al. [47]. If solute-solvent interactions are disregarded ($k_s, k_p \to 0$), the activity correction becomes negligible:

$$\lim_{k_s,k_p\to 0} \tilde{\gamma} = \lim_{k_s,k_p\to 0} \exp\left[k_s c_s(z,t) + k_p \sum_{j=1}^{n} c_j(z,t)\right] = 1 \tag{8}$$

in which the nGIEX model can be degenerated into the SMA model. The interaction parameters (k_s and k_p) differ significantly from the SMA model parameters (characteristic charge ν, equilibrium coefficient k_{eq}, shielding factor σ, and kinetic coefficient k_{kin}) in a crucial aspect: the interaction parameters lack subscripts, implying uniformity across all proteins.

At the adsorption equilibrium, $\partial q_i/\partial t = 0$, the static form of the nGIEX model is:

$$\frac{q_i}{c_i} = k_{eq,i}\left[\Lambda - \sum_{j=1}^{n}(\nu_j + \sigma_j)\cdot q_j\right]^{\nu_i} \cdot \exp\left(k_s c_s + k_p \sum_{j=1}^{n} c_j\right) \cdot c_s^{-\nu_i} \tag{9}$$

2.2. Experiments

In our previous study [41,48], we proposed a standardized approach for modeling ion-exchange chromatography. The approach guided the experimental design as follows:

1) Pulse-injection experiments and acid-base titration experiments were used for determining ε_t, D_{app} and Λ. The specific experimental methods were consistent with those of Chen, et al. [41]. System and column-specific parameters are listed as: $\varepsilon_t = 0.726$; $D_{app} = 0.404$ mm^2/s; $\Lambda = 0.389$ M.
2) Feed material was analyzed to determine the components considered for modeling. Fc-fusion proteins with a molecular weight of approximately 78 kDa and an isoelectric point of 8.7 were provided by Shanghai Henlius Biotech, Inc. (Shanghai, China.). The proteins were synthesized within Chinese hamster ovary cells and later purified utilizing protein A affinity chromatography. The eluate from the affinity chromatography was collected and stored at -80°C to preserve stability until required for subsequent study. The protein samples were analyzed by the whole-column imaged capillary isoelectric focusing (icIEF) system iCE3 (ProteinSimple, Silicon Valley, USA) and tested using a diode array detector within the 1260 infinity II liquid chromatography system (Agilent Technologies, Santa Clara, USA). Protein concentration was measured by high performance liquid chromatography using the POROS™ A 20 μm column with dimensions of 2.1 × 30 mm and a volume of 0.1 mL (Thermo Scientific, Waltham, USA). Components considered for modeling consisted of two acidic variants (A1 and A2), one main variant (M), and one basic variant (B), if only the components comprising over 5 % were included. The electropherogram illustrating the icIEF analysis of the feed material is depicted in Fig. 2.
3) The nGIEX model was calibrated by three gradient elution experiments with loading and elution conditions presented in Table 1. The sample was loaded at a concentration of 15.6 g/L. In these experiments, a flow rate of 2.78 mL/min was applied to a column with the height of 177 mm and the volume of 13.9 mL in an ÄKTA avant 25 system (Cytiva, Uppsala, Sweden). The column was packed with POROS™ XS 50 resin (Thermo Fisher Scientific, Waltham, USA). Formulation of the low-salt buffer A was 3.24 g/kg of $Na_2HPO_4{\cdot}12H_2O$ and 1.72 g/kg of $NaH_2PO_4{\cdot}2H_2O$, which was used for sample preparation, equilibration, and washing. Formulation of the high-salt buffer B was 3.94 g/kg of $Na_2HPO_4{\cdot}12H_2O$, 1.4 g/kg of $NaH_2PO_4{\cdot}2H_2O$, and 5.0 g/kg of NaCl, which was used for elution. All buffers were formulated with deionized water and filtered using a 0.2 μm sterile filter. The column was regenerated using a 1 M NaOH solution. Elution peaks exhibiting a UV signal exceeding 50 mAU at 280 nm were collected and analyzed. Analysis methods for the fractions were consistent with those used for the feed material.
4) Calibrated model's generalization ability was validated using process optimization at a loading of 20 g/L. Columns, samples, and buffer formulations used were consistent with those of the calibration experiments.

2.3. Chromatograms for evaluating dynamic Langmuirian/anti-Langmuirian behavior

Langmuirian/anti-Langmuirian elution types on chromatograms (dynamic adsorption) for both calibration and validation experiments can be identified by peak asymmetry, which is one intuitive representation of different adsorption types as depicted in Fig. 1. A skewness is considered as a crucial indicator for describing peak asymmetry [1], which can be calculated through moment analysis. A n-th raw moment and a n-th central moment are given by:

$$\mu_n' = \int_0^\infty t^n c(L,t)\mathrm{d}t \Big/ \int_0^\infty c(L,t)\mathrm{d}t \tag{10}$$

$$\mu_n = \int_0^\infty \left(t - \mu_1'\right)^n c(L,t)\mathrm{d}t \Big/ \int_0^\infty c(L,t)\mathrm{d}t \tag{11}$$

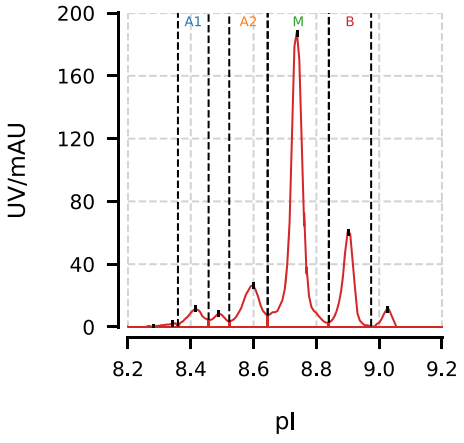

Fig. 2. Electropherogram for icIEF of feed material. Component contents: first acidic variants (A1) at 5.154 %, second acidic variants (A2) at 12.255 %, main variants (M) at 56.168 %, and basic (B) variants at 17.542 %.

Table 1
Experiment conditions of calibration and validation experiments.

No.	Purpose	Loading (g/L)	Elution condition
1	Calibration	20	Gradient 15 CV from 60 %B to 80 %B
2	Calibration	20	Gradient 25 CV from 60 %B to 80 %B
3	Calibration	30	Gradient 10 CV from 60 %B to 80 %B
4	Validation	20	Two-step 23.2 CV at 45.6 %B and 7.8 CV at 84 %B

The skewness can be calculated by:

$$\text{skewness} = \mu_3/\mu_2^{1.5} \tag{12}$$

A positive skewness indicates a tailing peak, corresponding to Langmuirian elution. Conversely, a negative skewness suggests the anti-Langmuirian elution.

2.4. Model calibration

An inverse method was chosen to estimate the nGIEX model parameters with an objection function as:

$$\min_{\nu,k_{\text{eq}},\sigma,k_{\text{kin}},k_{\text{s}},k_{\text{p}}} \sum_{j=1}^{m}\sum_{i=1}^{n} \frac{\| c_i^{\cdot}(t) - c_{h,i}(L,t;\nu_i,k_{\text{eq},i},\sigma,k_{\text{kin},i},k_{\text{s}},k_{\text{p}})\|_{L^2}^2}{\| c_i^{\cdot}(t)\|_{L^2}^2} \tag{13}$$

where m are the number of experiments, $\|\cdot\|_{L^2}$ is L^2-norm, $c_i^{\cdot}$ and $c_{h,i}$ are the experimented and simulated concentration of protein i in liquid phase, respectively.

In solving the optimization problem, we employed a two-step inverse method to enhance the efficiency and accuracy of the solution. Initially, we implemented a heuristic algorithm, specifically the differential evolution algorithm, which iterated 1600 times. Following this, we transitioned to a deterministic algorithm, the L-BFGS-B algorithm, to further refine the results. The convergence (early stopping) criterion for this algorithm was set such that the relative change in the gradient of the objective function was less than 10^{-5}. For these two algorithm, the search range for the nGIEX model parameters was defined as $\nu \in [1,20]$, $k_{\text{eq}} \in [10^{-6},10^{6}]$, $\sigma \in (0,200]$, $k_{\text{kin}} \in [10^{-12},1]$, $k_{\text{s}} \in [-20,0)$, and $k_{\text{p}} \in (0,10^{6}]$.

2.5. Isotherm sampling for evaluating static Langmuirian/anti-Langmuirian behavior

Sampling is referred to as evaluating the model performance across different parameter combinations. By performing sampling calculations on the static adsorption isotherms for each protein (with varying parameters), we can identify whether the static adsorption follows a Langmuirian or anti-Langmuirian pattern. Eq. (9) cannot be solved for multi-protein systems due to the inability to assess competitive adsorption among the proteins. Hence, only single-protein isotherm sampling was explored (in such situation, the nGIEX model equals to the GIEX model). Sampling was conducted at four salt concentrations: pure buffer A (0 % B), 60 % buffer B (initial gradient concentration), 70 % buffer B (peak position), and 80 % buffer B (final gradient concentration), with a protein concentration upper limit of 5 g/L.

2.6. Process optimization

To mitigate the risk of overfitting, we implemented process optimization as an external validation, which allows us to confirm that the model generalizes well to unseen data, thus enhancing its reliability. The process optimization identified an optimal two-step elution condition. This optimization task consists of two problems: the first optimization problem aimed to maximize the yield by finding the optimal elution conditions, while the second optimization problem aimed to maximize the yield by determining the optimal peak cut points, with the latter serving as a constraint for the former. This problem definition was adapted from Leweke and von Lieres [49] by modifying the first optimization problem.

The first optimization problem involves three decision variables: the salt concentration for the first step B_1, the salt concentration for the second step B_2, and the column volumes for the step switching $\text{CV}_{\text{switch}}$:

$$\begin{aligned} \max_{B_1,B_2,\text{CV}_{\text{switch}}} \quad & Y_{\text{product}}(c_i;B_1,B_2,\text{CV}_{\text{switch}},\ \text{CV}_{\text{L}},\text{CV}_{\text{R}}) \\ \text{s.t.} \quad & f(x) > 0 \\ & 0 \le B_1 < B_2 \le 100 \\ & 0 < \text{CV}_{\text{switch}} < \text{CV}_{\text{final}} \end{aligned} \tag{14}$$

where CV_{final} refers to the final column volume for the two-step elution (30 CV in this case), CV_{L} and CV_{R} respectively denote the left and right cut points. The constraint function $f(x)$ is defined as:

$$\begin{aligned} \max_{\text{CV}_{\text{L}},\text{CV}_{\text{R}}} \quad & f(x) = Y_{\text{product}}(c_i;\text{CV}_{\text{L}},\text{CV}_{\text{R}}) \\ \text{s.t.} \quad & P_{\text{product}} \ge 70\% \\ & P_{\text{A1}} + P_{\text{A2}} \le 10\% \\ & 0 \le \text{CV}_{\text{L}} < \text{CV}_{\text{R}} \le \text{CV}_{\text{final}} \end{aligned} \tag{15}$$

where the purity constraint was provided by Shanghai Henlius Biotech, Inc. and the purity and yield are defined as:

$$m_i(\text{CV}_{\text{L}},\text{CV}_{\text{R}}) = \int_{\text{CV}_{\text{L}}}^{\text{CV}_{\text{R}}} c_i(L,t)\mathrm{d}t \tag{16}$$

$$P_i(c_i) = \frac{m_i}{\sum_{j=1}^{n} m_j} \tag{17}$$

$$Y_i(c_i) = \frac{m_i}{c_{\text{inj},i}t_{\text{inj}}} \tag{18}$$

The two optimization problems employed the same optimization algorithms as those used for model calibration, specifically a combination of the differential evolution algorithm and the L-BFGS-B algorithm. The only difference lies in the search range of the decision variables, which has been clearly defined in Eq. (14).

2.7. Software and implementation

All coding works, including a numerical solution of the chromatographic models using a discontinuous Galerkin finite element method, a numerical integration in moment analysis, a differential evolution algorithm and a L-BFGS-B algorithm for model calibration and process optimization, and an implicit function solved in isotherm sampling, were implemented in Python. These computations were performed on an i9-13900K processor. For model calibration and process optimization, each computation was run three times with different random seeds, and the average results were taken to ensure that the obtained parameters are robust across different scenarios and to avoid local optimum. To reduce computational effort associated with the differential evolution algorithm, parallel computing techniques were employed.

3. Results

3.1. Anti-Langmuirian to Langmuirian elution behavior

The skewness, calculated from elution profiles and Eq. (12), was employed to differentiate the Langmuirian and anti-Langmuirian elution types. The obtained skewness is depicted in the legend of Fig. 3. It is observed across all charge variants that with an increase in retention volume, the skewness shows a transition from positive to negative. Additionally, the skewness of two acidic variants is positive (Langmuirian adsorption), whereas the skewness of main and basic variants is negative (anti-Langmuirian adsorption). A comparison between Fig. 3A and Fig. 3C reveals an increase in skewness for both main variant (-0.14

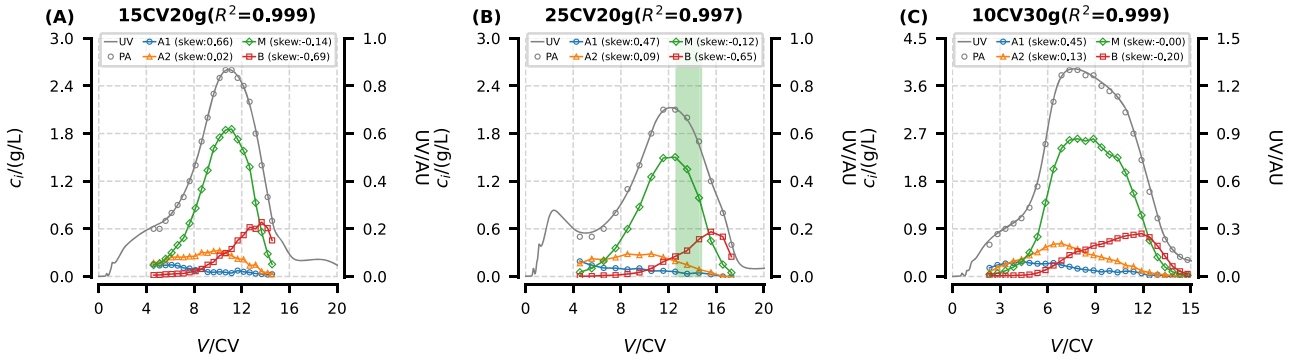

Fig. 3. Skewness of first acidic (A1), second acidic (A2), main (M), and basic (B) variants. R^2 in the title represents the agreement between protein amount (PA) of the collections and UV absorbance. Green area: the collection meeting the purity specifications. PA: protein amount.

to -0.12, then to -0.02) and basic variant (-0.69 to -0.65, then to -0.26) with an increase in loading volume. These results imply a weakening of the anti-Langmuirian adsorption, indicating a transition to the Langmuirian adsorption, which refers to as AL-L elution behavior. In contrast, the peak A1 exhibits L-AL elution behavior. This is likely due to computational errors resulting from the incomplete peak A1 and its concentrations falling below the detection limit, particularly in Fig. 3A.

3.2. Determination of the sign of interaction parameters

To describe the observed AL-L behavior, the multi-protein Mollerup activity model ($\tilde{\gamma} = e^{k_s c_s + k_p \sum_{j=1}^{n} c_j}$) proposed in our previous study [46] for describing the non-ideality of protein solution was introduced to the traditional SMA model, resulting in two additional interaction parameters to be determined, k_s and k_p. Prior to its applications, it was necessary to evaluate the sign of these two parameters, because there was some controversy in the literature regarding their sign [32,47]. In this work, we proposed that $k_s < 0$ and $k_p > 0$ by the following reasons:

With reference to Fig. 1, we evaluated the derivatives of the static form of the nGIEX model in Eq. (9) by taking limits. Considering c_i approaching positive infinity, Eq. (9) can be reduced to the SMA model with the expression and derivatives as:

$$\lim_{c_i \to \infty} q_i = k_{\mathrm{eq},i} \cdot \bar{q}_s^{\nu_i} \cdot c_s^{-\nu_i} \cdot c_i \tag{19}$$

$$\lim_{c_i \to \infty} \frac{\partial q_i}{\partial c_i} = \frac{\bar{q}_s^{\nu_i}}{k_{\mathrm{eq},i}^{-1} \cdot c_s^{\nu_i} + \nu_i \bar{q}_s^{\nu_i - 1} (\nu_i + \sigma_i) c_i} \tag{20}$$

$$\lim_{c_i \to \infty} \frac{\partial^2 q}{\partial c_i^2} = -\nu_i (\nu_i + \sigma_i) \frac{\bar{q}_s^{\nu_i - 1} (\nu_i + \sigma_i) c_i (\nu_i + 1) + 2 k_{\mathrm{eq},i}^{-1} \cdot c_s^{\nu_i}}{\bar{q}_s^{1 - 2\nu_i} \left[k_{\mathrm{eq},i}^{-1} \cdot c_s^{\nu_i} + \nu_i \bar{q}_s^{\nu_i - 1} (\nu_i + \sigma_i) c_i \right]^3} \tag{21}$$

Since the parameters of the SMA model (ν_i, $k_{\mathrm{eq},i}$, σ_i) are all positive, it can be deduced from Eqs. (20) and (21) that $\frac{\partial q_i}{\partial c_i} > 0$ and $\frac{\partial^2 q}{\partial c_i^2} < 0$. This indicates the Langmuirian adsorption behavior when c_i is sufficiently large. Conversely, when c_i approaches zero, the expression and derivatives of Eq. (9) become:

$$\lim_{c_i \to 0} q_i = k_{\mathrm{eq},i} \cdot \Lambda^{\nu_i} \cdot \tilde{\gamma} \cdot c_s^{-\nu_i} \cdot c_i \tag{22}$$

$$\lim_{c_i \to 0} \frac{\partial q_i}{\partial c_i} = k_{\mathrm{eq},i} \cdot \Lambda^{\nu_i} \cdot c_s^{-\nu_i} \cdot (k_p c_i + 1) \cdot \tilde{\gamma} = k_{\mathrm{eq},i} \cdot \Lambda^{\nu_i} \cdot c_s^{-\nu_i} \cdot \tilde{\gamma} \tag{23}$$

$$\lim_{c_i \to 0} \frac{\partial^2 q}{\partial c_i^2} = k_{\mathrm{eq},i} \cdot \Lambda^{\nu_i} \cdot c_s^{-\nu_i} \cdot (k_p c_i + 2) k_p \cdot \tilde{\gamma} = k_{\mathrm{eq},i} \cdot \Lambda^{\nu_i} \cdot c_s^{-\nu_i} \cdot 2 k_p \cdot \tilde{\gamma} \tag{24}$$

As mentioned previously, the comparison between Fig. 3A and Fig. 3C indicates the anti-Langmuirian adsorption at low c_i. According to Fig. 1, $\frac{\partial q_i}{\partial c_i} > 0$ and $\frac{\partial^2 q}{\partial c_i^2} > 0$ for anti-Langmuirian adsorption. To satisfy these conditions, k_p must be positive. Constrained by the range of activity coefficients, k_s is negative; otherwise, the activity would consistently exceed one.

3.3. Model calibration

After determining the sign of k_s and k_p, an inverse method was employed to calibrate the proposed nGIEX model as defined by Eq. (13). To streamline the calibration process, it was assumed that charge variants exhibited similar properties apart from their differing charges. Therefore, the SMA parameter σ was unity for different variants, which aligns with numerous studies utilizing the inverse method to fit SMA formalism [50–53]. Similarly, the interaction parameters k_s and k_p lack subscripts, implying uniformity across all variants.

Based on these assumptions, the six isotherm parameters ν, k_{eq}, σ, k_{kin}, k_s, and k_p can be divided into two categories: ν, k_{eq}, and k_{kin} differing based on variant types, and σ, k_s, and k_p uniform across all variants. In this study, a total of four variants required modeling, resulting in 15 degrees of freedom. The optimal model parameters were obtained through numerous iterations, as presented in Table 2.

By comparing ν of different variants, it is evident that this parameter exhibits an increasing trend with the peak position. This implies that in cation exchange chromatography, variants eluted later have a higher charge, indicating stronger binding affinity to the ligand. σ is 12.41, suggesting that due to steric mass action, around 12.41 binding sites are shielded. This shielding effect leads to the Langmuirian adsorption in the nGIEX model at high loadings. k_s and k_p are -8.46 and 28488 M^{-1}, respectively, which is consistent with the order of magnitude reported by Huuk, et al. [47], Koch, et al. [32] and Nfor, et al. [35]. A negative k_s and a positive k_p indicates that an increase in salt concentration or a decrease in protein concentration can result in a reduction in solution activity.

The elution curves simulated with the determined model parameters are illustrated in Fig. 4. As mention previously, the skewness of elution curves concluded that variants A1 and A2 exhibited the Langmuirian adsorption (positive skewness), whereas variants M and B demonstrated the anti-Langmuirian adsorption (negative skewness). Fig. 4 shows that

Table 2
nGIEX model parameters determined by inverse method of first acidic (A1), second acidic (A2), main (M), and basic (B) variants.

Variant	ν	$k_{eq} \times 10^4$	σ	$k_{kin} \times 10^7/(sM^{\nu})$	k_s/M^{-1}	k_p/M^{-1}
A1	5.40	91.15	12.41	5165.67	-8.46	28488
A2	6.86	15.68		176.70		
M	7.28	12.08		34.45		
B	8.23	4.51		4.45		

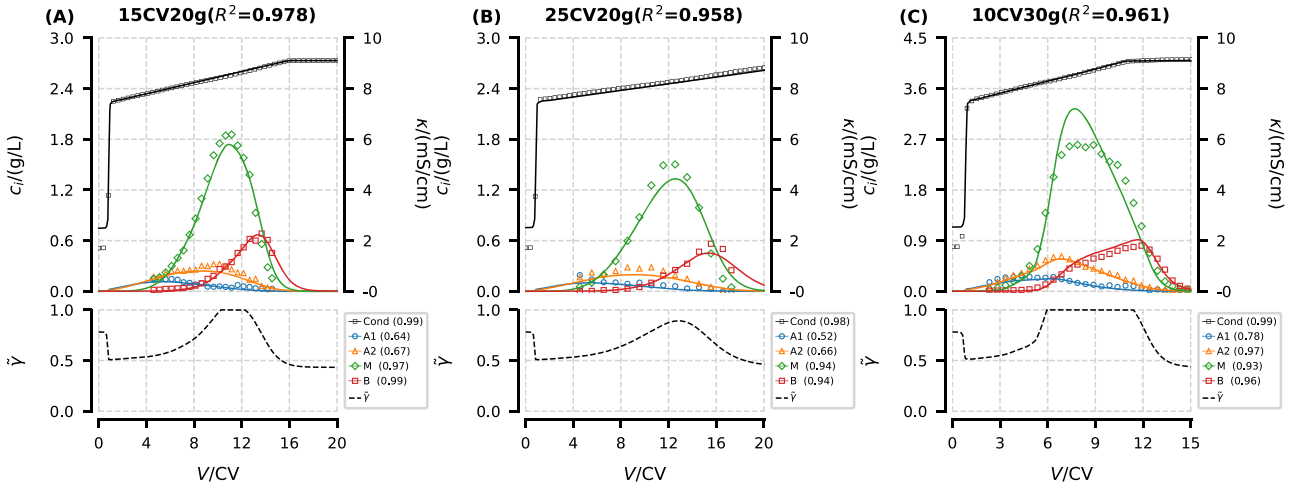

Fig. 4. Chromatograms and activity models of linear gradient elution experiments with elution starting at 0 CV for model calibration. R^2 in the title represents the agreement between experiments (scatters) and model simulations (lines) of first acidic (A1), second acidic (A2), main (M), and basic (B) variants.

R^2 between model simulations and experiments consistently exceeded 0.95. This satisfactory fit suggests that the nGIEX model is capable of simultaneously simulating the Langmuirian and anti-Langmuirian adsorption for all variants.

An intuitive observation supporting this suggestion can be seen in Fig. 4C, where the experiment was conducted with a gradient length of 10 CV with a loading of 30 g/L. The variants M and B exhibits pronounced anti-Langmuirian adsorption, resulting in asymmetric peaks. The developed nGIEX model adequately can capture this asymmetry (R^2 is 0.961). The asymmetric peaks simulated with the nGIEX model resemble those derived from other more sophisticated mechanistic models [29,31–33,42,47]. These studies attributed such asymmetry to AL-L behavior, especially pronounced under high loading conditions. This perspective is corroborated in our study, as particularly evident in Fig. 4C (loading at 30 g/L), where the asymmetry of peaks is much pronounced. This is because multi-layer adsorption occurs only when the loading reaches a sufficiently high level. Although the models proposed in these literatures were based on different theories, they all considered activity corrections for protein solutions [29,31–33,42,47]. Therefore, it can be inferred that our findings owe to the introduction of activity correction in the nGIEX model.

The difference of variant M in Fig. 4C may be due to the relatively high loading, limiting the mass transfer and causing the assumption of the equilibrium dispersive model to no longer hold. As a result, the overserved peaks are lower while the simulations do not account for this limitation, leading to higher simulated peaks. It is undeniable that the low concentrations of side components fall below the detection limits of the analytical method, leading to incomplete peaks and reduced fitting quality, as illustrated by the acidic and basic variants in Fig. 4A-B.

The curves of activity model composed of k_s and k_p are illustrated in Fig. 4. Due to $k_s < 0$ and $k_p > 0$, the activity coefficients exhibit a negative correlation with salt concentration but a positive correlation with protein concentration. The equilibrium buffer utilized in this study had an ionic strength of 0.029 M. With the calculation of the activity model in Eq. (6), its activity coefficient is 0.8, indicating that the equilibrium buffer used is a negative bias solution ($\tilde{\gamma} < 1$). As the gradient starts, 80 % of buffer B is introduced into the column, causing a rise in salt concentration and a decrease in activity coefficients. Upon protein elution, there is an upward trend in activity coefficients, which results in a delayed elution of peaks, generating fronting peaks akin to those in anti-Langmuirian adsorption as depicted in Fig. 1.

3.4. Isotherm sampling

In addition to evaluating the AL-L elution behavior (dynamic adsorption), the nGIEX model's ability to describe sigmoidal isotherms (static adsorption) was assessed for each variant through isotherm sampling. This assessment was based on the nGIEX model parameters listed in Table 2.

Results of the isotherm sampling are depicted in Fig. 5. The adsorption at the pure buffer A exhibits strong Langmuirian adsorption. For the adsorption isotherms containing a certain proportion of buffer B, anti-Langmuirian adsorption at low concentrations and Langmuirian adsorption at high concentrations could be found, indicating the sigmoidal isotherms (AL-L adsorption). Khalaf, et al. [29] argued that the point at which the behavior shifts from anti-Langmuirian to Langmuirian significantly impacts the adsorption process. This shifting point is dependent on the salt concentration in the mobile phase. An increase in salt concentration could shift the point to occur at higher mobile-phase concentrations.

A comparison of the four subplots in Fig. 5 reveals that at the same mobile-phase concentration, the stationary-phase concentrations for variants A1, A2, M, and B increase sequentially, implying that their peak positions in chromatograms also increase sequentially. Furthermore, under the same conditions, the areas of the anti-Langmuirian adsorption region for variants M and B are larger than those for variants A1 and A2, indicating that variants M and B have more tendency to undergo anti-Langmuirian adsorption. In Fig. 3, we did not observe anti-Langmuirian elution behavior for variants A1 and A2, but it is evident in Fig. 5. This discrepancy primarily arises from the isotherm sampling targeting single-protein systems, thus overlooking interactions between proteins. This implies that the plotted adsorption isotherms for single proteins differ from those of multiple proteins.

Through the isotherm sampling, it is confirmed that the developed nGIEX model exhibits the sigmoidal adsorption isotherms, thus possessing the capability to describe AL-L elution behavior. This is attributed to the introduction of the activity correction term. Vetter and Strube [23] have reported that the SAS model with consideration of the activity correction can exhibit sigmoidal isotherms.

3.5. Process optimization

The above sections confirmed that the nGIEX model can describe AL-L elution behavior (dynamic adsorption) and the sigmoidal isotherm (static adsorption), its extrapolability was further externally validated through process optimization. Prior to process optimization, we

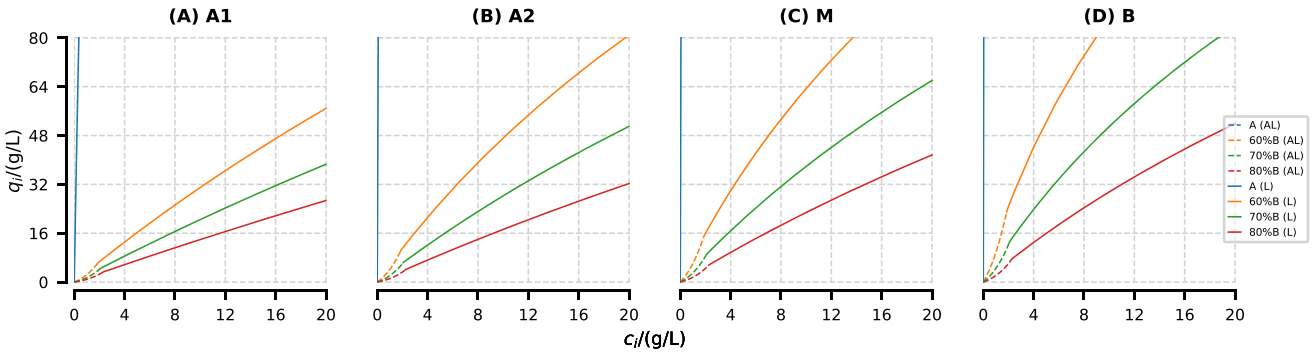

Fig. 5. Sampling of nGIEX isotherm model of first acidic (A1), second acidic (A2), main (M), and basic (B) variants. AL: anti-Langmuirian. L: Langmuirian.

calculated the yield of variant M in three calibration experiments while meeting specifications as defined in Eq. (15). Only the experiment with a gradient length of 25 CV and a loading of 20 g/L (Fig. 3B) achieved a yield of 25.9 % within the purity specifications, with a collection range of 18.7-20.7 CV.

Solving the problem as defined by Eqs. (14) and (15) yielded the optimal two-step elution conditions (Table 1): a first step with a salt concentration of 45.6 % buffer B and an elution volume of 23.2 CV, followed by a second step with a salt concentration of 84 % buffer B and an elution volume of 7.8 CV. The collection range satisfying the purity specification is 24.6-28.0 CV, with the predicted yield of 86.7 %.

Based on the optimal elution conditions predicted by the model, a two-step elution experiment was performed. The resulting protein amount comparison, chromatograms, and activity models are presented in Fig. 6A-B. The yield from the curves of protein amount in Fig. 6A was calculated within the predicted collection range, which resulted in a yield of 89.1 %, close to the predicted value of 86.7 %. We observed characteristics of the optimal elution conditions predicted from the model: the salt concentration in the first step should elute acidic peaks without eluting variant M (these peaks were not collected due to their concentrations being below the detection limit, but their concentrations could be estimated from the UV signal), while the salt concentration in the second step should elute variant M without eluting variant B. It was this elution characteristic that raised the yield from 25.9 % to 89.1 %.

The skewness of the four variants was calculated as shown in Fig. 6A. An increase in skewness for variants M and B was observed compared to the calibration experiments in Fig. 3. The skewness of variant M changed from negative (anti-Langmuirian adsorption in Fig. 3) to positive (Langmuirian adsorption in Fig. 6A), reaffirming the existence of AL-L elution behavior.

The elution curves predicted by the developed nGIEX model are shown in Fig. 6B. The variant M, as predicted by the model, exhibits tailing peaks indicative of Langmuirian adsorption, consistent with experimental observations. Fig. 6 shows that R^2 between model predictions and experiments for elution curves is 0.942, which indicates that the nGIEX model calibrated under anti-Langmuirian adsorption can also predict its Langmuirian adsorption under high salt concentrations.

The process optimization based on the nGIEX model demonstrates excellent predictive capabilities when applied to high loadings for industrial applications, confirming the rationality of calibrating the nGIEX model. Through this model-based optimization, the yield increased from 25.9 % before optimization to 89.1 % after optimization. Compared to traditional design of experiments methods, model-based process optimization offers a deeper understanding of the chromatography process. This effectively reduces costs in process development and achieves a more globally optimal process.

4. Discussion

The nGIEX model developed in this work can describe the AL-L

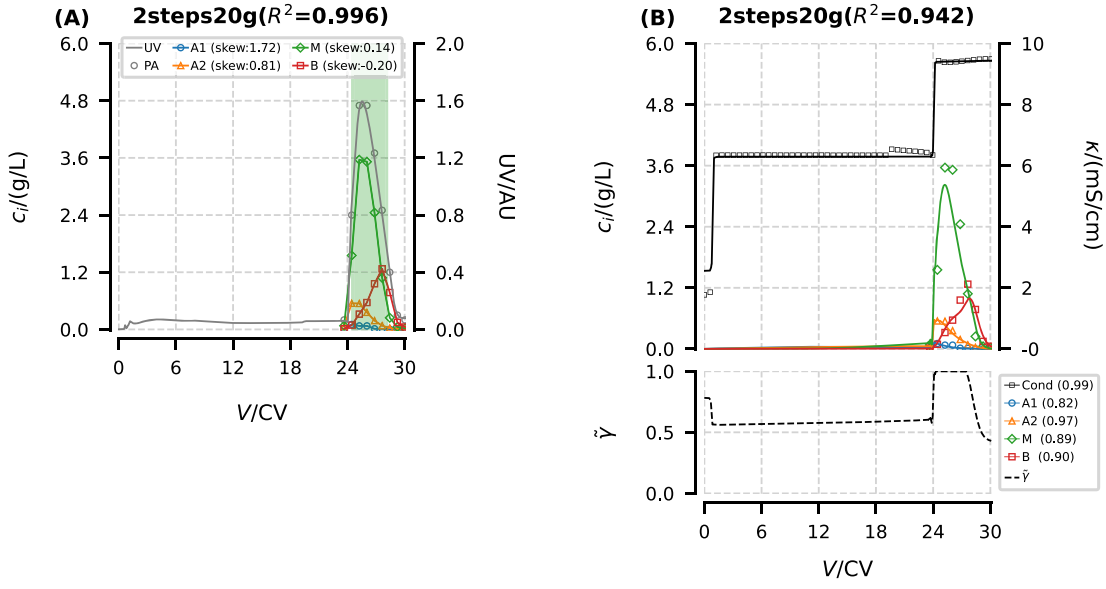

Fig. 6. Protein amount comparison (a), chromatogram and activity model (b) of two-step experiment (scatters) and model prediction (lines) with elution starting at 0 CV for process optimization. A1: first acidic, A2: second acidic, M: main, and B basic variants. Green area: the collection meeting the purity specifications.

behavior observed in both dynamic and static adsorption of industrial Fc-fusion proteins due to the introduction of the activity correction ($\widetilde{\gamma} = \exp\left(k_s c_s + k_p \sum_{j=1}^{n} c_j\right)$). This AL-L behavior cannot be described by the traditional SMA model (purely Langmuirian model). In the chromatograms (Fig. 4 and Fig. 6), $\widetilde{\gamma} = 1$ at the peak position, where the nGIEX model is equivalent to the SMA model. However, the key point of our model is its ability to describe the anti-Langmuirian behavior, which is common at low mobile-phase concentrations where the nGIEX model differs from the SMA model ($\widetilde{\gamma} < 1$).

This activity correction is based on the thermodynamically consistent multi-protein Mollerup model proposed in our previous work [46]. The summation in the activity model implies that our activity model considers the contributions of all proteins to the solution activity, which aligns better with the thermodynamic definition of activity. The nGIEX model differs significantly from the reported GIEX model in describing multi-component AL-L elution behavior, as demonstrated through numerical experiments in our previous work [46].

The performance of the multi-protein Mollerup model is influenced by the sign of the two interaction parameters. The model can describe the AL-L behavior only when $k_s < 0$ and $k_p > 0$. As analyzed in Eqs. (20), (21), (23), and (24), a negative k_s and a positive k_p suggests the anti-Langmuirian adsorption ($\frac{\partial q_i}{\partial c_i} > 0$ and $\frac{\partial^2 q}{\partial c_i^2} > 0$) as c_i approaches zero, while the Langmuirian adsorption ($\frac{\partial q_i}{\partial c_i} > 0$ and $\frac{\partial^2 q}{\partial c_i^2} < 0$) as c_i tends to positive infinity. The combination of these two adsorption types gives a sigmoid isotherm. This inference is consistent with the activity model introduced by Koch, et al. [32] for polypeptide separation via cation exchange chromatography, but contradicts the findings of Huuk, et al. [47], who inferred negative values for both parameters in their study on antibody separation via cation exchange chromatography and therefore did not observe AL-L behavior in their isotherm sampling. The sign of the interaction parameters are subject to debate, appearing not only in cation exchange chromatography but also in hydrophobic interaction chromatography [54] and mixed-mode chromatography [35,37,55].

In addition to considering the impact of the asymmetric activity model $\widetilde{\gamma}$ itself, it is essential to consider the role of $\widetilde{\gamma}$ in the isotherm model from two perspectives: the practical thermodynamic equilibrium constants $k_{eq,i}\widetilde{\gamma}$ and the corrected protein binding capacity $\overline{q}_s^{\nu_i}\widetilde{\gamma}$.

The first perspective is adsorption equilibrium. We can perceive the introduced activity coefficients as corrections to the equilibrium coefficient in Eq. (4), where the corrected equilibrium coefficient is $k_{eq,i}\widetilde{\gamma}$. $k_s < 0$ indicates that a reduction in salt concentration leads to an increase in equilibrium coefficients, while $k_p > 0$ indicates that a growth in protein concentration leads to an increase in equilibrium coefficients. The increase in equilibrium coefficients intensifies the adsorption process in equilibrium, while diminishing the desorption process. This implies that the protein-ligand interaction is strengthened, making it more difficult for proteins to dissociate from ligands, thereby resulting in delayed protein elution. The corrected equilibrium coefficients $k_{eq,i}\widetilde{\gamma}$ were named as practical thermodynamic equilibrium constants in the literature [30,56,57]. When evaluating adsorption equilibrium, practical thermodynamic equilibrium constants ($k_{eq,i}\widetilde{\gamma}$) should be considered rather than $k_{eq,i}$ alone, which varies over several orders of magnitude between the four variants as shown in Table 2.

The second perspective is protein binding capacity. If we express the product of the Langmuirian term ($\left[\Lambda - \sum_{j=1}^{n}(\nu_j + \sigma_j)q_j\right]^{\nu_i}$) and the anti-Langmuirian term ($\exp\left(k_s c_s + k_p \sum_{j=1}^{n} c_j\right)$) in Eq. (4), $\overline{q}_s^{\nu_i}\widetilde{\gamma}$, as the protein binding capacity, $k_s < 0$ implies a decrease in protein binding capacity with an increase in salt concentration, consistent with the understanding that proteins bind to the ligand at low salt concentrations and elute at high salt concentrations. $k_p > 0$ indicates an increase in protein binding capacity with an increase in protein concentration, suggesting the occurrence of a multi-layer adsorption process. Khalaf, et al. [29] and Mollerup, et al. [30] also utilized the multi-layer adsorption to explain the AL-L elution behavior.

The developed nGIEX model demonstrates excellent predictive capabilities when applied to high loadings for industrial applications. It holds promise as the next-generation chromatographic model, capable of simultaneously meeting academic demands for thermodynamic consistency and industrial requirements in everyday project work. The AL-L behavior was observed in several industrial projects involving different separation systems, not limited to cation-exchange chromatographic separation of charge variants of Fc-fusion proteins in this work, indicating that the AL-L behavior is a common phenomenon for industrial applications. Developing a thermodynamically consistent model to describe this behavior has profound implications for industrial applications. However, this work primarily provides a model-based explanation of this phenomenon, observations of multi-layer adsorption require further experimental design and exploration.

5. Conclusion

In this study, AL-L elution behavior was observed in cation-exchange chromatographic separation of charge variants of industrial Fc-fusion proteins. The multi-protein Mollerup activity model was integrated into the traditional SMA model to characterize this behavior, resulting in a new model named as the nGIEX model. The signs of two additional model parameters were determined by taking their limits ($k_s < 0$ and $k_p > 0$). The model was calibrated by three linear gradient elution experiments. $R^2 > 0.95$ indicates the nGIEX model can effectively describe the AL-L elution behavior (dynamic adsorption). Using isotherm sampling, the nGIEX model exhibited sigmoidal AL-L isotherms (static adsorption) for all variants. The model's extrapolation capability was externally validated through process optimization, resulting in an optimal two-step elution condition and a yield improvement of the main variant from 25.9 % to 89.1 % while meeting purity specifications (>70 %). We also discussed the reasons why the nGIEX model can describe AL-L behavior from two perspectives: practical thermodynamic equilibrium constants and the corrected protein binding capacity. This work confirms that the nGIEX model holds promise as the next-generation chromatographic model, capable of simultaneously meeting academic demands for thermodynamic consistency and industrial requirements in everyday project work.

CRediT authorship contribution statement

Yu-Cheng Chen: Writing – original draft, Visualization, Validation, Software, Resources, Methodology, Investigation, Funding acquisition, Formal analysis, Data curation, Conceptualization. **Xue-Zhao Zhong:** Writing – review & editing, Methodology, Investigation, Data curation. **Ce Shi:** Writing – review & editing, Methodology, Investigation. **Ran Chen:** Writing – review & editing, Resources, Project administration. **Mattia Sponchioni:** Writing – review & editing, Supervision. **Shan-Jing Yao:** Writing – review & editing. **Dong-Qiang Lin:** Writing – review & editing, Supervision, Project administration, Funding acquisition, Conceptualization.

Declaration of competing interest

The authors declare that they have no known competing financial interests or personal relationships that could have appeared to influence the work reported in this paper.

Acknowledgments

This work was supported by National Natural Science Foundation of China (22078286), Zhejiang Key Science and Technology Project (2023C03116), National Key R&D Program of China

(2021YFE0113300), and China Scholarship Council (CSC, no. 202306320355).

Supplementary materials

Supplementary material associated with this article can be found, in the online version, at doi:10.1016/j.chroma.2024.465602.

Data availability

Data available within the article or its supplementary materials.

References

[1] S. Yamamoto, K. Nakanishi, R. Matsuno, Ion-exchange chromatography of proteins, 1 ed., Taylor & Francis, 1988.

[2] G. Carta, A. Jungbauer, Introduction to protein chromatography, Protein Chromatography, Wiley, Weinheim, Germany, 2020, pp. 63–91.

[3] D.-Q. Lin, Y.-C. Chen, X.-Y. Chen, S.-J. Yao, Exploration and practice of online–offline blended teaching in process simulation courses, J. Chem. Educ. 101 (2024) 1966–1973, https://doi.org/10.1021/acs.jchemed.4c00095.

[4] A. Tiwari, V.S. Masampally, A. Agarwal, A.S. Rathore, Digital twin of a continuous chromatography process for mAb purification: Design and model-based control, Biotechnol. Bioeng. 120 (2023) 748–766, https://doi.org/10.1002/bit.28307.

[5] C. Ding, M. Ierapetritou, Machine learning-based optimization of a multi-step ion exchange chromatography for ternary protein separation, Comput. Chem. Eng. 184 (2024) 108642, https://doi.org/10.1016/j.compchemeng.2024.108642.

[6] W.R. Keller, S.T. Evans, G. Ferreira, D. Robbins, S.M. Cramer, Understanding the effects of system differences for parameter estimation and scale-up of high throughput chromatographic data, J. Chromatogr. A 1661 (2022) 462696, https://doi.org/10.1016/j.chroma.2021.462696.

[7] S.H. Altern, A.J. Kocot, J.P. LeBarre, C. Boi, M.W. Phillips, D.J. Roush, S. Menegatti, S.M. Cramer, Mechanistic model-based characterization of size-exclusion-mixed-mode resins for removal of monoclonal antibody fragments, J. Chromatogr. A 1718 (2024) 464717, https://doi.org/10.1016/j.chroma.2024.464717.

[8] S. Bhoyar, V. Kumar, M. Foster, X. Xu, S.J. Traylor, J. Guo, A.M. Lenhoff, Predictive mechanistic modeling of loading and elution in protein A chromatography, J. Chromatogr. A 1713 (2024) 464558, https://doi.org/10.1016/j.chroma.2023.464558.

[9] Y. Qu, I. Baker, J. Black, L. Fabri, S.L. Gras, A.M. Lenhoff, S.E. Kentish, Application of mechanistic modelling in membrane and fiber chromatography for purification of biotherapeutics — A review, J. Chromatogr. A 1716 (2024) 464588, https://doi.org/10.1016/j.chroma.2023.464588.

[10] T.C. Silva, M. Eppink, M. Ottens, Digital twin in high throughput chromatographic process development for monoclonal antibodies, J. Chromatogr. A 1717 (2024) 464672, https://doi.org/10.1016/j.chroma.2024.464672.

[11] L.K. Shekhawat, A. Tiwari, S. Yamamoto, A.S. Rathore, An accelerated approach for mechanistic model based prediction of linear gradient elution ion-exchange chromatography of proteins, J. Chromatogr. A 1680 (2022) 463423, https://doi.org/10.1016/j.chroma.2022.463423.

[12] C.Y. Ding, H. Ardeshna, C. Gillespie, M. Ierapetritou, Process design of a fully integrated continuous biopharmaceutical process using economic and ecological impact assessment, Biotechnol. Bioeng. 119 (2022) 3567–3583, https://doi.org/10.1002/bit.28234.

[13] Y.-C. Chen, X.-Y. Chen, Z.-Y. Lin, S.-J. Yao, D.-Q. Lin, Practical teaching of modeling tools for ion-exchange chromatography: A case study, J. Chem. Educ. 100 (2023) 3888–3896, https://doi.org/10.1021/acs.jchemed.3c00439.

[14] Y.-C. Chen, R.-Q. Mao, S.-J. Yao, D.-Q. Lin, Continuous ion-exchange chromatography for protein polishing and enrichment, in: P.N. Nesterenko, C. F. Poole, Y. Sun (Eds.), Ion-Exchange Chromatography and Related Techniques, Elsevier, 2024, pp. 535–552.

[15] H. Narayanan, M. von Stosch, F. Feidl, M. Sokolov, M. Morbidelli, A. Butté, Hybrid modeling for biopharmaceutical processes: advantages, opportunities, and implementation, Front. Chem. Eng. 5 (2023), https://doi.org/10.3389/fceng.2023.1157889.

[16] H. Narayanan, M. Luna, M. Sokolov, A. Butté, M. Morbidelli, Hybrid models based on machine learning and an increasing degree of process knowledge: application to cell culture processes, Ind. Eng. Chem. Res. 61 (2022) 8658–8672, https://doi.org/10.1021/acs.iecr.1c04507.

[17] H. Narayanan, T. Seidler, M.F. Luna, M. Sokolov, M. Morbidelli, A. Butté, Hybrid Models for the simulation and prediction of chromatographic processes for protein capture, J. Chromatogr. A 1650 (2021) 462248, https://doi.org/10.1016/j.chroma.2021.462248.

[18] C.Y. Ding, C. Gerberich, M. Ierapetritou, Hybrid model development for parameter estimation and process optimization of hydrophobic interaction chromatography, J. Chromatogr. A 1703 (2023) 464113, https://doi.org/10.1016/j.chroma.2023.464113.

[19] S.-Y. Tang, Y.-H. Yuan, Y.-C. Chen, S.-J. Yao, Y. Wang, D.-Q. Lin, Physics-informed neural networks to solve lumped kinetic model for chromatography process, J. Chromatogr. A 1708 (2023) 464346, https://doi.org/10.1016/j.chroma.2023.464346.

[20] S.G. Subraveti, Z. Li, V. Prasad, A. Rajendran, Can a computer "learn" nonlinear chromatography?: Physics-based deep neural networks for simulation and optimization of chromatographic processes, J. Chromatogr. A 1672 (2022) 463037, https://doi.org/10.1016/j.chroma.2022.463037.

[21] V. Chopda, A. Gyorgypal, O. Yang, R. Singh, R. Ramachandran, H.R. Zhang, G. Tsilomelekis, S.P.S. Chundawat, M.G. Ierapetritou, Recent advances in integrated process analytical techniques, modeling, and control strategies to enable continuous biomanufacturing of monoclonal antibodies, J. Chem. Technol. Biotechnol. 97 (2022) 2317–2335, https://doi.org/10.1002/jctb.6765.

[22] C.Y. Ding, M. Ierapetritou, A novel framework of surrogate-based feasibility analysis for establishing design space of twin-column continuous chromatography, Int. J. Pharm. 609 (2021) 121161, https://doi.org/10.1016/j.ijpharm.2021.121161.

[23] F.L. Vetter, J. Strube, Need for a next generation of chromatography models-academic demands for thermodynamic consistency and industrial requirements in everyday project work, Processes 10 (2022) 715, https://doi.org/10.3390/pr10040715.

[24] H. Narayanan, M. Sponchioni, M. Morbidelli, Integration and digitalization in the manufacturing of therapeutic proteins, Chem. Eng. Sci. 248 (2022) 117159, https://doi.org/10.1016/j.ces.2021.117159.

[25] C.A. Brooks, S.M. Cramer, Steric mass-action ion-exchange - displacement profiles and induced salt gradients, AIChe J. 38 (1992) 1969–1978, https://doi.org/10.1002/aic.690381212.

[26] Y.-C. Chen, S.-J. Yao, D.-Q. Lin, Parameter-by-parameter method for steric mass action model of ion exchange chromatography: Theoretical considerations and experimental verification, J. Chromatogr. A 1680 (2022) 463418, https://doi.org/10.1016/j.chroma.2022.463418.

[27] Y.-C. Chen, S.-J. Yao, D.-Q. Lin, Parameter-by-parameter method for steric mass action model of ion exchange chromatography: Simplified estimation for steric shielding factor, J. Chromatogr. A 1687 (2023) 463655, https://doi.org/10.1016/j.chroma.2022.463655.

[28] K. Mihlbachler, M.A. De Jesús, K. Kaczmarski, M.J. Sepaniak, A. Seidel-Morgenstern, G. Guiochon, Adsorption behavior of the (±)-Tröger's base enantiomers in the phase system of a silica-based packing coated with amylose tri (3,5-dimethyl carbamate) and 2-propanol and molecular modeling interpretation, J. Chromatogr. A 1113 (2006) 148–161, https://doi.org/10.1016/j.chroma.2006.02.001.

[29] R. Khalaf, B.C. de Neuville, M. Morbidelli, Protein adsorption in polyelectrolyte brush type cation-exchangers, J. Chromatogr. A 1471 (2016) 126–137, https://doi.org/10.1016/j.chroma.2016.10.024.

[30] J.M. Mollerup, T.B. Hansen, S.S. Frederiksen, A. Staby, Thermodynamic modeling of chromatographic separation, in: E. Grushka, N. Grinberg (Eds.), Advances in Chromatography, 2010, pp. 57–97.

[31] F. Seelinger, F. Wittkopp, T. von Hirschheydt, C. Frech, Anti-Langmuir elution behavior of a bispecific monoclonal antibody in cation exchange chromatography: Mechanistic modeling using a pH-dependent Self-Association Steric Mass Action isotherm, J. Chromatogr. A 1689 (2023) 463730, https://doi.org/10.1016/j.chroma.2022.463730.

[32] J. Koch, D. Scheps, M. Gunne, O. Boscheinen, M. Hafner, C. Frech, Mechanistic modeling and simulation of a complex low and high loading elution behavior of a polypeptide in cation exchange chromatography, J. Sep. Sci. 45 (2022) 2008–2023, https://doi.org/10.1002/jssc.202200098.

[33] J. Koch, D. Scheps, M. Gunne, O. Boscheinen, C. Frech, Mechanistic modeling of cation exchange chromatography scale-up considering packing inhomogeneities, J. Sep. Sci. 46 (2023) 2300031, https://doi.org/10.1002/jssc.202300031.

[34] Y.-X. Yang, Y.-C. Chen, S.-J. Yao, D.-Q. Lin, Parameter-by-parameter estimation method for adsorption isotherm in hydrophobic interaction chromatography, J. Chromatogr. A 1716 (2024) 464638, https://doi.org/10.1016/j.chroma.2024.464638.

[35] B.K. Nfor, M. Noverraz, S. Chilamkurthi, P. Verhaert, L.A.M. van der Wielen, M. Ottens, High-throughput isotherm determination and thermodynamic modeling of protein adsorption on mixed mode adsorbents, J. Chromatogr. A 1217 (2010) 6829–6850, https://doi.org/10.1016/j.chroma.2010.07.069.

[36] T. Hahn, N. Geng, K. Petrushevska-Seebach, M.E. Dolan, M. Scheindel, P. Graf, K. Takenaka, K. Izumida, L. Li, Z. Ma, N. Schuelke, Mechanistic modeling, simulation, and optimization of mixed-mode chromatography for an antibody polishing step, Biotechnol. Prog. 39 (2023) e3316, https://doi.org/10.1002/btpr.3316.

[37] S.H. Altern, J.P. Welsh, J.Y. Lyall, A.J. Kocot, S. Burgess, V. Kumar, C. Williams, A. M. Lenhoff, S.M. Cramer, Isotherm model discrimination for multimodal chromatography using mechanistic models derived from high-throughput batch isotherm data, J. Chromatogr. A 1693 (2023) 463878, https://doi.org/10.1016/j.chroma.2023.463878.

[38] R. Hess, D. Yun, D. Saleh, T. Briskot, J.-H. Grosch, G. Wang, T. Schwab, J. Hubbuch, Standardized method for mechanistic modeling of multimodal anion exchange chromatography in flow through operation, J. Chromatogr. A 1690 (2023) 463789, https://doi.org/10.1016/j.chroma.2023.463789.

[39] K. Arkell, M.P. Breil, S.S. Frederiksen, B. Nilsson, Mechanistic modeling of reversed-phase chromatography of insulins with potassium chloride and ethanol as mobile-phase modulators, ACS. Omega 2 (2017) 136–146, https://doi.org/10.1021/acsomega.6b00248.

[40] K. Arkell, M.P. Breil, S.S. Frederiksen, B. Nilsson, Mechanistic modeling of reversed-phase chromatography of insulins within the temperature range 10-40 degrees C, ACS. Omega 3 (2018) 1946–1954, https://doi.org/10.1021/acsomega.7b01527.

[41] Y.-C. Chen, H.L. Lu, R.Z. Wang, G. Sun, X.Q. Zhang, J.Q. Liang, A. Jungbauer, S. J. Yao, D.Q. Lin, Standardized approach for accurate and reliable model development of ion-exchange chromatography based on parameter-by-parameter method and consideration of extra-column effects, Biotechnol. J. 19 (2024) 2300687, https://doi.org/10.1002/biot.202300687.
[42] F. Seelinger, F. Wittkopp, T. von Hirschheydt, C. Frech, Application of the Steric Mass Action formalism for modeling under high loading conditions: Part 2. Investigation of high loading and column overloading effects, J. Chromatogr. A 1676 (2022) 463266, https://doi.org/10.1016/j.chroma.2022.463266.
[43] F. Seelinger, F. Wittkopp, T. von Hirschheydt, M. Hafner, C. Frech, Application of the steric mass action formalism for modeling under high loading conditions: Part 1. Investigation of the influence of pH on the steric shielding factor, J. Chromatogr. A 1676 (2022) 463265, https://doi.org/10.1016/j.chroma.2022.463265.
[44] J.M. Mollerup, Applied thermodynamics: A new frontier for biotechnology, Fluid. Phase Equilib. 241 (2006) 205–215, https://doi.org/10.1016/j.fluid.2005.12.037.
[45] J.M. Prausnitz, R.N. Lichtenthaler, E.G. De Azevedo, Molecular thermodynamics of fluid-phase equilibria, Pearson Education, 1998.
[46] Y.-C. Chen, S.-J. Yao, D.-Q. Lin, Enhancing thermodynamic consistency: Clarification on the application of asymmetric activity model in multi-component chromatographic separation, J. Chromatogr. A 1731 (2024) 465156, https://doi.org/10.1016/j.chroma.2024.465156.
[47] T.C. Huuk, T. Hahn, K. Doninger, J. Griesbach, S. Hepbildikler, J. Hubbuch, Modeling of complex antibody elution behavior under high protein load densities in ion exchange chromatography using an asymmetric activity coefficient, Biotechnol. J. 12 (2017) 1600336, https://doi.org/10.1002/biot.201600336.
[48] Y.-C. Chen, G. Recanati, F. De Mathia, D.Q. Lin, A. Jungbauer, Residence time distribution in continuous virus filtration, Biotechnol. Bioeng. 121 (2024) 1876–1888, https://doi.org/10.1002/bit.28696.
[49] S. Leweke, E. von Lieres, Chromatography analysis and design toolkit (CADET), Comput. Chem. Eng. 113 (2018) 274–294, https://doi.org/10.1016/j.compchemeng.2018.02.025.
[50] T. Hahn, A. Sommer, A. Osberghaus, V. Heuveline, J. Hubbuch, Adjoint-based estimation and optimization for column liquid chromatography models, Comput. Chem. Eng. 64 (2014) 41–54, https://doi.org/10.1016/j.compchemeng.2014.01.013.
[51] V. Kumar, S. Leweke, E. von Lieres, A.S. Rathore, Mechanistic modeling of ion-exchange process chromatography of charge variants of monoclonal antibody products, J. Chromatogr. A 1426 (2015) 140–153, https://doi.org/10.1016/j.chroma.2015.11.062.
[52] T. Hahn, T. Huuk, A. Osberghaus, K. Doninger, S. Nath, S. Hepbildikler, V. Heuveline, J. Hubbuch, Calibration-free inverse modeling of ion-exchange chromatography in industrial antibody purification, Eng. Life Sci. 16 (2016) 107–113, https://doi.org/10.1002/elsc.201400248.
[53] F. Rischawy, D. Saleh, T. Hahn, S. Oelmeier, J. Spitz, S. Kluters, Good modeling practice for industrial chromatography: Mechanistic modeling of ion exchange chromatography of a bispecific antibody, Comput. Chem. Eng. 130 (2019) 14, https://doi.org/10.1016/j.compchemeng.2019.106532.
[54] S. Andris, J. Hubbuch, Modeling of hydrophobic interaction chromatography for the separation of antibody-drug conjugates and its application towards quality by design, J. Biotechnol. 317 (2020) 48–58, https://doi.org/10.1016/j.jbiotec.2020.04.018.
[55] H.G. Bock, D.H. Cebulla, C. Kirches, A. Potschka, Mixed-integer optimal control for multimodal chromatography, Comput. Chem. Eng. 153 (2021) 107435, https://doi.org/10.1016/j.compchemeng.2021.107435.
[56] J.M. Mollerup, The thermodynamic principles of ligand binding in chromatography and biology, J. Biotechnol. 132 (2007) 187–195, https://doi.org/10.1016/j.jbiotec.2007.05.036.
[57] J.M. Mollerup, A review of the thermodynamics of protein association to ligands, protein adsorption, and adsorption isotherms, Chem. Eng. Technol. 31 (2008) 864–874, https://doi.org/10.1002/ceat.200800082.